The influence of channel cross section shape in speech production

B. Wu et A. Van Hirtum
GIPSA-lab, 11 rue des Mathématiques, 38402 Saint Martin D'Hères Cedex, France
annemie.van-hirtum@gipsa-lab.grenoble-inp.fr

Pressure–driven channel flow is associated with speech production. Constricted channel portions occur either naturally during articulation or are due to a pathology or an abnormality. Quasi one-dimensional or two-dimensional flow models has proven to be extremely useful to grasp the underlying physics, despite the dimensional reduction. Since the channel is assumed to be either rectangular or circular, details of the cross section shape perpendicular to the main flow direction are neglected. Nevertheless, thanks to advanced imaging techniques, it is well known that cross-sections shapes of constricted laryngeal or vocal tract portions during speech production deflect from circular or rectangular. The viscous contribution to the flow depends on the cross section shape, so that neglection of cross-section details can be questioned. In the current work, a simple quasi-three dimensional flow model is proposed which accounts for the kinetic inertia, viscosity as well as the cross section shape in case of laminar viscous flow. Experiments are performed to characterize the influence of the cross section shape on steady flow through constricted channel. Numerical results are obtained using immersed boundary method. Finally, a comparison is made between modeled, experimental and simulated data.

1 Introduction

Pressure–driven channel flow is associated with physiological flows for which constricted channel portions occur either naturally or are due to a pathology or an abnormality. Well known examples are for instance airflow through the human lower (asthma) or upper airways (human speech production, obstructive sleep apnea) and blood flow through a stenosis.

Consequently, efforts are made to model pressure–driven flow through constricted channels in order to understand the mechanisms involved and to develop aiding tools for health care workers. Due to the complexity of the human respiratory and cardiovascular system, most studies severely simplify the physiological reality in order to come up with a configuration depending on a limited number of meaningful physiological and physical parameters. Such a simplification enhances understanding of the ongoing physical phenomena and facilitates experimental validation of the models accuracy.

In general, simplifications of the flow model through portions of the respiratory or cardiovascular system are based on a non dimensional analysis of the governing Navier-Stokes equations while accounting for typical values of physiological, geometrical and flow characteristics [5]. From these observations relevant non-dimensional numbers (Mach number Ma, Reynolds number Re, Strouhal number Sr and mean channel width-to-height ratio Ar) allow one to simplify the flow model. For instance, glottal flow during phonation can be assumed to be incompressible, laminar inviscid, quasi-steady and two-dimensional [1]. The assumption of a two-dimensional glottal flow implies a rectangular glottal cross section shape for which height $h(x)$ varies along main flow direction x, whereas glottal width w is fixed. Theoretical flow models based on these assumptions result in a quasi-one-dimensional flow description when accounting for kinetic losses as well as viscous losses. Therefore, quasi-one-dimensional (1D) or two-dimensional (2D) flow models have proven to be extremely useful to grasp the underlying physics and are applied to mimic and predict ongoing phenomena using few computational resources while allowing experimental validation on replicas with different degrees of complexity.

Nevertheless, the assumption of a 1D or 2D geometry implies that details of the cross section shape perpendicular to main flow direction x are neglected. Since the cross section shape is known to affect boundary layer development, varying the cross section shape might alter the viscous contribution to the pressure drop, the theoretical flow models using the above mentioned simplifications can thus be questioned for normal as well as pathological geometrical conditions [6]. Moreover, the computational load of accurate three-dimensional modeling, requiring a large amount of mesh points, should not be underestimated and seems at current date out of reach for clinical applications [4].

So the aim of the current work is to assess the potential impact of a simple 'quasi-three-dimensional' flow model – with low computational cost and which takes into account kinetic losses, viscosity as well as the cross section shape – on the flow outcome. The flow model outcome is analyzed with respect to the outcome of a quasi-one-dimensional, a two-dimensional flow model, a three-dimensional flow model, experimental flow data as well as numerical data.

2 Quasi-three-dimensional model

For a given fluid under the assumption of pressure–driven, steady, laminar and incompressible flow, the streamwise momentum equation of the governing Navier-Stokes equation is approximated using volume flow rate conservation $dQ/dx = 0$, as:

$$-\frac{Q^2}{A^3}\frac{dA}{dx} + \frac{1}{\rho}\frac{dP}{dx} = \nu\left(\frac{\partial^2 u}{\partial y^2} + \frac{\partial^2 u}{\partial z^2}\right), \qquad (1)$$

with driving pressure gradient dP/dx, cross section area A, local velocity $u(x, y, z)$, volume flow rate Q, fluid density ρ (1.2kg/m^3) and kinematic viscosity ν ($1.5\times10^{-5}\text{m}^2/\text{s}$ for air). The flow model expressed in (1) accounts for viscosity (right hand term) as well as flow inertia (first source term at the left hand side) and depends therefore on the area as well as on the shape of the cross section. It is seen that for a uniform channel, so that $dA/dx = 0$ holds, (1) reduces to purely viscous flow [6]. The same way, it is seen that when viscosity is neglected, *i.e.* $\nu = 0$ as for an ideal (symbol B) inviscid flow, (1) reduces to Euler's equation (Bernoulli flow).

For uniform geometries and applying the no-slip boundary condition $u = 0$ on the channel walls, (1) can be rewritten as a classical Dirichlet problem which can be solved analytically for simple cross section shapes, such as the geometries shown in Fig. 2. Therefore, exact solutions are obtained for: local velocity $u(x, y, z)$, local pressure $p(x)$, wall shear stress τ, volume flow rate Q and bulk Reynolds number $Re = \frac{QD}{\nu A}$ with hydraulic diameter D [6].

In the following, a uniform constricted channel of internal diameter 25mm with an abrupt diverging area portion is accounted for, in which a uniform constriction with fixed length $L_c = 25mm$ and varying cross section shape is inserted, as depicted in Fig. 1. For an abrupt expansion characterized by

a sharp trailing edge, the streamwise position of flow separation x_s is fixed and coincides with the trailing end of the constriction, so that $x_s = x_3$. The pressure downstream from the flow separation point is assumed to be zero so that $P_d = 0$ holds for $x \geq x_s$ and the model outcome remains constant for $x \geq x_s$. Consequently, imposing the upstream pressure P_0 allows to impose the total driving pressure difference.

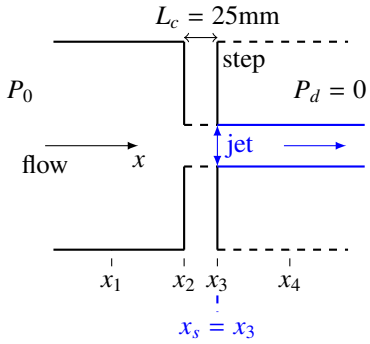

Figure 1: Flow through an abrupt expansion.

3 Cross section shapes

In order to use the cross section shape in quasi-analytical models only shapes for which the geometry can be expressed analytically are assessed: circle (cl), rectangle (re), ellipse (el), and circular sector (cs) [6]. Different cross section shapes are illustrated in Fig. 2.

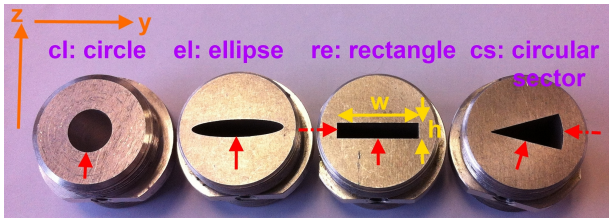

Figure 2: Illustration of experimentally assessed uniform cross section shapes and position of the pressure taps P_1 (full arrow) and P_2 (dashed arrow): front view of the cross section shapes along the (y, z) plane.

The chosen shapes have, although a severe idealization, some relevance to describe the channel cross section shape in the case of normal as well as pathological geometrical conditions of the human respiratory (and even cardiovascular systems). The cross section is positioned in the (y, z) plane where y denotes the spanwise and z the transverse direction. The cross section shapes have constant area $A_c = 79\text{mm}^2$. The corresponding geometrical characteristics are summarized in Table 1: hydraulic diameter D, width w and height h.

4 Experimental setup

Flow facility and pressure measurements The experimental setup, depicted in Fig. 3, consists of an air compressor (Atlas Copco GA7), followed by a pressure regulator (Norgren type 11-818-987) providing an airflow at constant pressure. The volume flow rate is controlled by a manual valve

Table 1: Overview of geometrical parameters: hydraulic diameter D, width w, height h, cross section area A_c and constriction length L_c.

	cl	cs	el	re
D [mm]	10	7.2	6.7	6.6
w [mm]	10	17.3	22.4	19.8
h [mm]	10	9.0	4.5	4.0

$A_c = 79\text{mm}^2$, $L_c = 25\text{mm}$

placed downstream from the pressure regulator. The volume flow rate is measured by a thermal mass flow meter (Model 4043 TSI) with an accuracy of 2% of its reading. To homogenize the flow, a settling chamber is used, with dimensions 0.25m×0.3m×0.35m, to which a series of 3 perforated plates with holes of diameter 1.5mm are added. The walls of the settling chamber are tapered with acoustic foam (SE50-AL-ML Elastomeres Solutions) in order to avoid acoustic resonances. The influence of the cross section shape on the flow development is assessed experimentally by adding one of the constricted channel portions, illustrated in Fig. 2, to a uniform circular tube, with unconstricted internal diameter 25mm. The flow channel is mounted to the settling chamber by means of a converging nozzle. The used nozzle and resulting nozzle flow is detailed in [2]. Pressure sensors (Kulite XCS-093) can be positioned in pressure taps of diameter 0.4mm upstream from (P_0) and in the middle of (P_1 and P_2) the constricted portion illustrated in Fig. 2. Except for the air compressor, the whole setup is placed in a confined room in order to avoid flow disturbances. Electrical signals are amplified and conditioned using a pre-amplifier/conditioning board (National Instruments SXCI-1121) connected to a PC through a National Instruments BNC-2080 and a National Instruments PCI-MIO-16XE acquisition card. The acquired data are processed using LabView 7 software (National Instruments).

Volume flow rate Q and Pressure sensors P are sampled at 500Hz and 24kHz, respectively. Statistical quantities, such as mean values, are derived on 5s of steady signal for the measured volume flow rate $Q(t)$ and pressure signal $P(t)$. Flow experiments are performed for volume rates within the range $0 \leq Q \leq 200$l/min. The increment is 5l/min for $Q \leq 80$l/min, 10l/min for 90l/min$\leq Q \leq 100$l/min and 25l/min for $Q \geq 125$l/min.

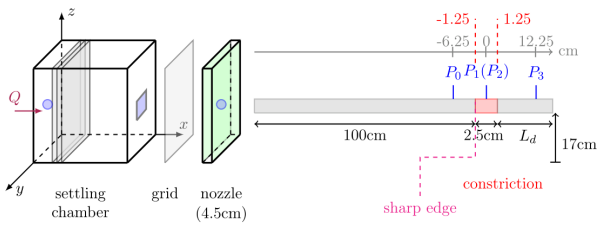

Figure 3: Schematic overview of the experimental setup in pressure measurements.

Velocity measurements The flow velocity immediately downstream from the constriction is measured for different cross section shapes by hot film anemometry. The inlet of the constriction is characterized by a sharp edge. The setup is detailed in Fig. 4. The hot film (TSI 1201-20) is mounted to a home-made positioning system providing a positioning accuracy of 0.1mm. The probe displacement is controlled by a user-defined matrix implemented in LabView (National Instruments). At each spatial measurement position, the hot-film output voltage is sampled at 10kHz during 40s for which the mean and root mean square velocity is derived.

Transverse velocity profiles are gathered by positioning the hot film at a distance < 1mm downstream from the center of the nozzle exit and displacing the hot film with a transverse step of 0.5mm parallel to the cross section exit plane across the directions shown in Fig. 5. Longitudinal velocity profiles in the near field downstream from the constriction are obtained by positioning the hot film at a distance < 1mm downstream from the center of the nozzle exit and displacing the hot film with streamwise steps of 1mm up to 1cm downstream from its initial position followed by a streamwise step of 5mm up to 8cm from its initial position.

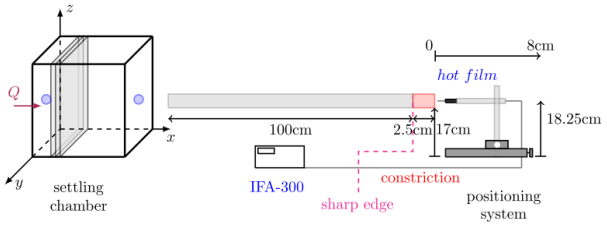

Figure 4: Illustration of the experimental configuration used to measure the velocity field immediately downstream from the constriction.

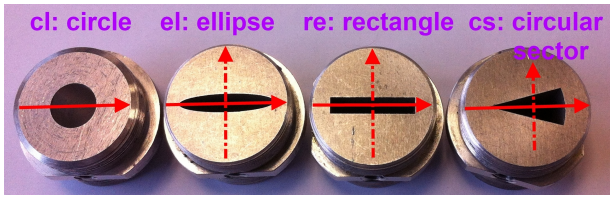

Figure 5: Experimentally assessed directions along the major axis (full arrow) and along the minor axis (dashed arrow) for transverse velocity profiles.

5 Simulation

The immersed boundary method [3] is applied to describe steady pressure-driven flow through a constricted channel. A geometrical model of the channel structure is generated using the SolidWorks CAD software, and the resulting CAD structure is converted into a mesh with tetrahedron cells. The constricted channel has a total length $L_z = 22.5$cm with radius $r_x = 1.25$cm at the inlet and outlet. The constricted portion is of length $L_c = 2.5$cm with cross section area 0.79cm^2. The unconstricted upstream portion has length $L_u = 5$cm and the unconstricted downstream portion has length $L_d = 15$cm. The channel walls are rigid and have a thickness of 0.1cm. The structure is immersed in a rectangular 5.4cm×5.4cm×22.5cm fluid box shown in Fig. 6.

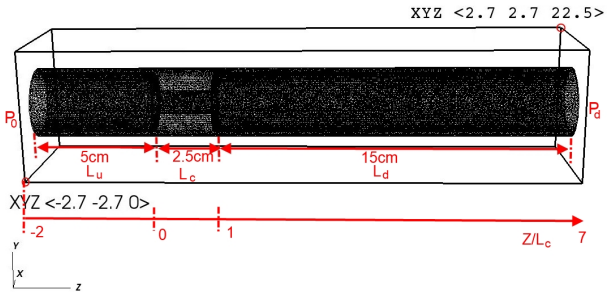

Figure 6: Illustration of the structure immersed in a 5.4cm×5.4cm×22.5cm rectangular fluid box for which two corner points coordinates are given [cm]. The streamwise direction corresponds to the normalized Z direction.

In the current simulations, we initialize the discretization of the fluid box with a $N \times N \times N$ Cartesian grid for $N = 128$. A pressure gradient is prescribed between the inlet ($Z/L_c = -2$) and outlet ($Z/L_c = 7$) of the interior part of the flow channel, *i.e.* $P_0 - P_d$, whereas zero pressure boundary conditions are employed along the remainder of the fluid domain boundary. The fluid is air with density $\rho = 1.2$kg/m^3 and dynamic viscosity $\mu = 1.8 \times 10^{-5}$Pa·s. Simulations for different cross section shapes are performed for $P_0 = 35$Pa and the downstream pressure is fixed to $P_d = 0$Pa.

6 Results

6.1 Experimental data

The pressure distribution in a constricted channel with fixed streamwise area is experimentally assessed for steady flow. The measured pressure P_1 and normalized pressure P_1/P_0 are shown in Fig. 7. It is seen that the mean values within the constriction vary up to 20% of P_0, which confirms the need to take into account the cross section shape. And a minimum value is observed for all cross section shapes for $2000 \leq Re \leq 4000$ immediately followed by a maximum. The exact position of minimum depends on the Reynolds number. Indeed, this range of Reynolds numbers is likely to associated with the transition form laminar flow to turbulent flow. Further research is needed to fully determine the flow dynamics.

Fig. 8 illustrates the measured normalized mean velocity as a function of the cross section shape for sharp edges at the constriction inlet. The impact of the cross section shape on the near field is apparent for all assessed volume flow rates with respect to the initial velocity u_0, the extent of the potential cone as with respect to its initial decay. The initial velocity at the constriction exit for instance is seen to vary up to 20%. The same way as for the pressure measurements, the measured velocity profiles suggest that the flow behavior is shaped by the sharp edges and the presence of flow structures. Indeed, the decreasing tendency of the velocity within the potential cone suggests jet forcing due to the sharp edges at the constriction inlet.

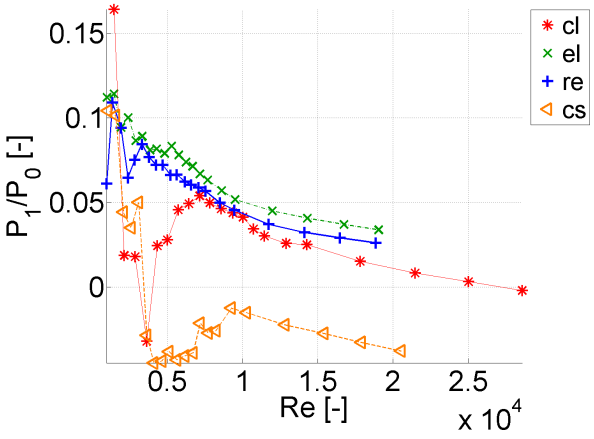

Figure 7: Measured mean pressures within the constriction normalized pressure measured within the constriction as a function of Reynolds number $P_1/P_0(Re)$ for L_u = 1m without (L_d = 0cm) downstream pipe.

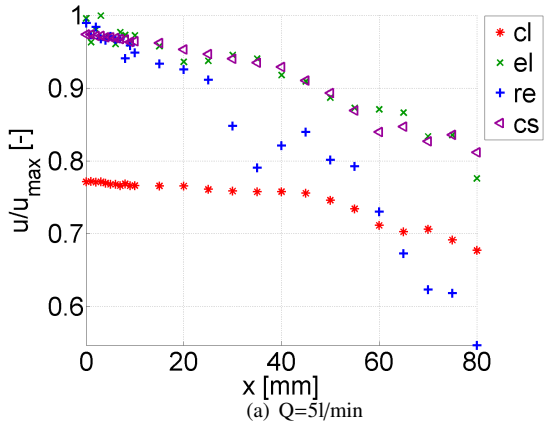

(a) Q=5l/min

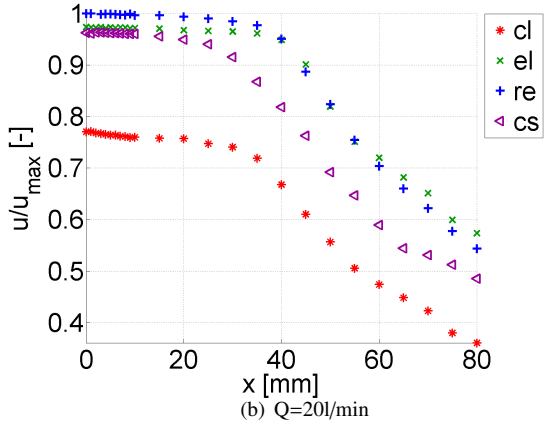

(b) Q=20l/min

Figure 8: Measured near field normalized longitudinal mean velocity profiles u/u_{max} along the centerline of the jet as a function of volume flow rate Q for sharp edges at the constriction inlet. u_{max} denotes the maximum mean velocity for all cross section shapes for a given volume flow rate.

6.2 Numerical data

Fig. 9 and Fig. 10 illustrate simulated (IB) and modeled (mod) streamwise pressure and velocity distributions for P_0 = 35Pa. Distributions are shown for a circular, elliptical, rectangular and circular sector cross section shape. The modeled pressure distribution shown in Fig. 9 results from the quasi-three-dimensional model. For the IB method, the streamwise pressure distribution in Fig. 9 is obtained by sampling instantaneous values for each streamwise Z position at the transverse (X,Y) position associated with the maximum velocity in the analytical model assuming viscous developed flow through the constricted channel. Fig. 10 illustrates the modeled (mod) and simulated (IB) local streamwise bulk velocity obtained as the transverse mean velocity. The modeled values are sampled at the same transfers (X,Y) position whereas the transverse velocity profile is obtained from the volume flow rate Q_{mod} resulting from the quasi-three-dimensional flow model to compute the velocity distribution along the constricted portion assuming developed viscous flow.

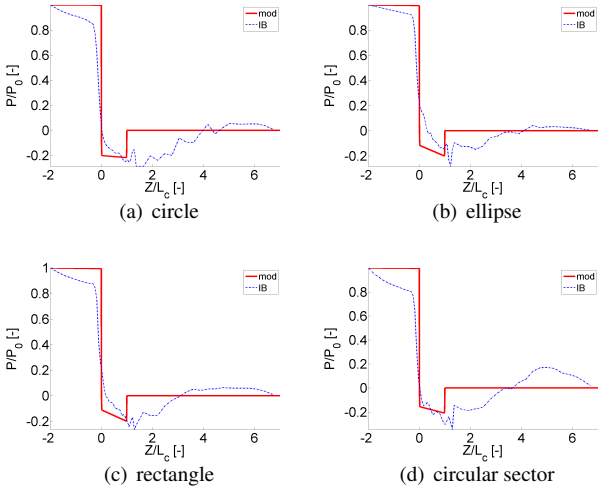

(a) circle (b) ellipse (c) rectangle (d) circular sector

Figure 9: Streamwise pressure distributions obtained using the quasi-three-dimensional model (mod) and the instantaneous simulated pressure distribution using the immersed boundary method (IB).

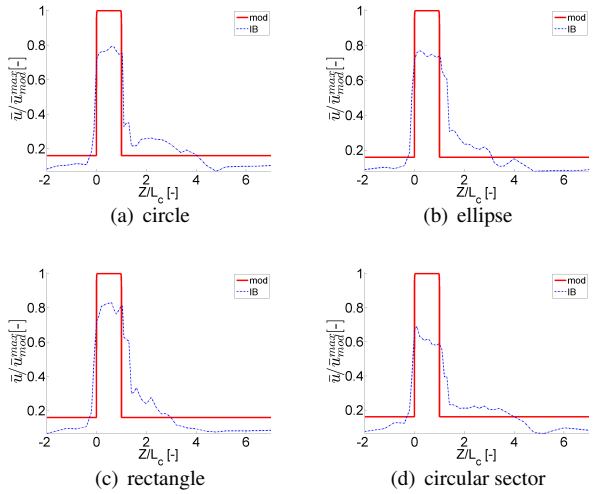

(a) circle (b) ellipse (c) rectangle (d) circular sector

Figure 10: Modeled (mod) and simulated (IB) streamwise mean or local bulk velocity distributions are normalized by the maximum modeled local bulk velocity $\bar{u}_{mod}^{max}$.

Fig. 9 shows that within the constriction both the quasi-three-dimensional model and the simulated pressure distribution are decreasing and result in negative pressures. In general, the quasi-three-dimensional model provides a good approximation of the simulated pressure within the constriction since an overall difference of 5% between simulated and

modeled pressure distribution is found. This motivates the use of the quasi-three-dimensional flow model to compute the fluid forces on the wall within the constriction while accounting for the cross section shape. On the other hand, it is seen that the quasi-three-dimensional model is incapable to account for jet reattachment downstream from the constriction. Consequently, the simplified quasi-three-dimensional model is not able to capture the pressure distribution downstream from the constriction. This is a major drawback of the proposed quasi-three-dimensional flow model and as a consequence the quasi-three-dimensional model underestimates the pressure difference immediately downstream from the constriction with 20% or more.

The main findings of comparing the modeled and simulated streamwise pressure distribution holds also when comparing the modeled and simulated mean streamwise velocity as seen from Fig. 10. Indeed, within the constriction, the modeled mean velocities overestimate the simulated values with maximum 30% and minimum 15%, whereas immediately downstream from the constriction the error increases since no reattachment is accounted for in the quasi-three-dimensional flow model.

6.3 Model validation

Fig. 11 illustrates the measured and modeled normalized pressures within the constriction P_1/P_0 as a function of the pressure upstream from the constriction P_0. It is seen that for all assessed shapes the variation of the normalized model outcome accounting for the cross section shape is within 10%. Since the constriction is uniform all modeled values result in a positive prediction of the pressure within the constriction and a continuously decreasing ratio P_1/P_0 for increasing P_0. Consequently, none of the assessed flow models is capable to accurately predict the measured negative pressures within the constriction or the extrema observed for the measured pressure within the transition regime $2000 \leq Re \leq 4000$. Both phenomena result from more complex flow phenomena which are unaccounted for in the used flow models. They are likely triggered by the sharp edges at the inlet of the constriction. Nevertheless, the discrepancy between modeled and measured values is quantified.

In addition to the model accounting for the exact cross section shape (mod), Fig. 11 depicts the two-dimensional and axisymmetrical boundary layer model (Th) and quasi-one-dimensional model (BP). For the rectangular cross section shape it is seen that the quasi-three-dimensional model outcome and the quasi-one-dimensional model outcome are a good match (< 3%). The two-dimensional boundary model (Th2D) provides the most accurate prediction $P_0 > 30$Pa (< 3%) and up to 7% for $P_0 < 30$Pa. The quasi-three-dimensional model outcome provides accurate match for all the pressure P_0 (< 7%). In case of the circular cross section shape, the axisymmetrical boundary layer model (ThAxi) result in good approximation (< 5%) for $P_0 > 50$Pa and the quasi-three-dimensional model leads to 5% accuracy for $P_0 > 10$Pa. In general, the accuracy of the quasi-three-dimensional model compared to the measured data is summarized as < 6% for $P_0 > 50$Pa and up to 12% for $P_0 < 50$Pa depending on the cross section shape.

Measurements of the mean transverse velocity profile at the exit of the constriction in absence of a downstream pipe, offers (besides the pressure measurements within the constriction) an opportunity to further consider the relevance and limitations of the proposed quasi-three-dimensional model partly exploiting fully developed flow. Indeed, the measured volume flow rate Q allows to estimate the velocity distribution assuming fully developed viscous flow. A comparison is made between modeled and measured transverse profiles along the 'major' and 'minor' axis defined in Fig. 5. Examples of measured and modeled profiles for different volume flow rates along the 'major' and 'minor' axis of the constriction with rectangular cross section are presented in Fig. 12.

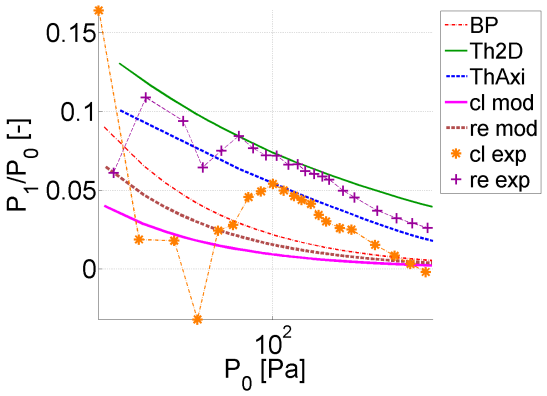

Figure 11: Normalized measured and modeled pressures within the constriction P_1/P_0 as a function of upstream pressure P_0: circular (cl) and rectangular (re) cross section shape. Modeled values are obtained from the outcome of the quasi-three-dimensional (mod), quasi-one-dimensional (BP) and boundary layer solution (ThAxi for circular and Th2D for rectangular).

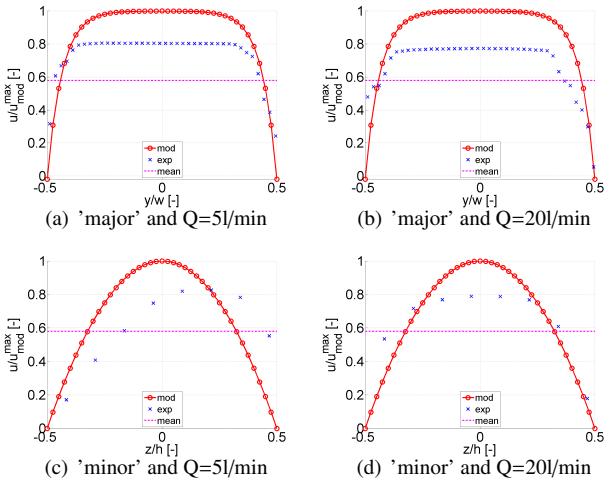

(a) 'major' and Q=5l/min (b) 'major' and Q=20l/min

(c) 'minor' and Q=5l/min (d) 'minor' and Q=20l/min

Figure 12: Modeled (mod) and mean measured (exp) transverse velocity profiles along the 'major' and 'minor' axis normalized by the maximum modeled velocity u_{mod}^{max} at the exit of constriction for rectangular cross section for different volume flow rates Q. As a reference the bulk velocity $\bar{u}$ is indicated. The transverse coordinate (y or z) is normalized by the total width $y_{tot} = w$ of the constricted portion.

In general, for both the 'major' and 'minor' axis, it is observed that the modeled and measured transverse profiles matches well within the boundary layer. However, since the modeled profile is fully developed, it tends to overestimate

the velocity for the core flow enveloped by the boundary layers. Given that the simplified model does not accounts for complex flow dynamics, which based on the presented experimental results suggested to contribute to the flow development – such as vortex generation, vortex interaction or turbulence – at first sight the comparison is surprisingly good.

In order to further quantify the model accuracy with respect to measured transverse profiles shown in Fig. 12, the following relative overall error is used:

$$\mathrm{err} = \frac{\sqrt{\frac{1}{n}\sum_{n}\left(u_{exp}(n) - u_{mod}(n)\right)^2}}{\bar{u}} \times 100, \qquad (2)$$

where u_{mod} and u_{exp} denote the modeled velocity and mean measured velocities respectively for n measuring positions and $\bar{u}$ denotes the bulk velocity at the constriction exit.

The resulting overall error (2) between modeled and experimental transverse velocity profiles along the 'major' and 'minor' axis is illustrated in Fig. 13 for the rectangular constriction shape as a function of the volume flow rate Q. It is seen that the relative error varies between 25% and 50% of the bulk velocity. The variation of the error with the volume flow rate is more pronounced for velocity profiles along the 'major' axis than along the 'minor' axis. Note that for the profiles along the 'major' axis a maximum error is retrieved for 50l/min.

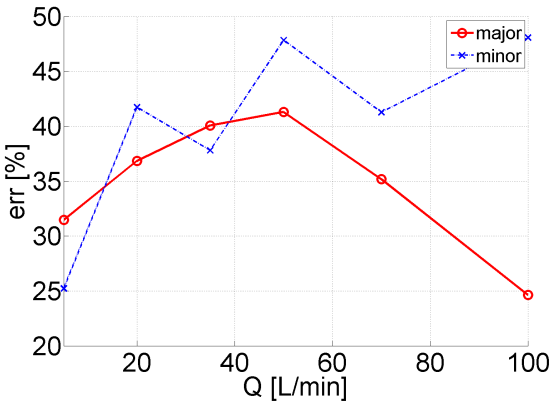

Figure 13: Illustration of the overall error (2) between modeled and experimental transverse velocity profiles along the 'major' and 'minor' axis of the rectangular cross section for different volume flow rates Q.

7 Conclusion

The impact of the cross section shape on flow through a constricted channel is shown for modeled, experimental and numerical data. Pressure measurements within the constriction show that the flow model provides 6% accurate pressure prediction for $P_0 > 50$Pa. The transverse velocity profiles show that the predicted profiles using the quasi-three-dimensional flow model, although not accurate, do provide some main characteristics of the velocity profile such as the asymmetrical development of the boundary layers in the case of asymmetrical geometries. On the other hand, it is shown that the proposed flow model can not capture the complexity of the flow dynamics. Moreover, the model outcome is compared to the outcome of the numerical simulation of a laminar incompressible three-dimensional flow model. It is seen that predictions obtained from the model are suitable to predict the order of magnitude of flow quantities within the constriction whereas predictions downstream from the constriction are useless. The simulated flow field on the other hand is shown to capture some of the flow dynamics at a high computational cost.

8 Acknowledgments

This work has been partially supported by LabEx PERSYVAL-Lab (ANR-11-LABX-0025-01).

References

[1] J. Cisonni, A. Van Hirtum, X. Pelorson, and J. Willems. Theoretical simulation and experimental validation of inverse quasi one-dimensional steady and unsteady glottal flow models. *Journal of the Acoustical Society of America*, 124:535–545, 2008.

[2] X. Grandchamp, Y. Fujiso, B. Wu, and A. Van Hirtum. Steady laminar axisymmetrical nozzle flow at moderate reynolds numbers: modeling and experiment. *Journal of Fluids Engineering*, 134(1):011203, 2012.

[3] B.E. Griffith and X.Y. Luo. Hybrid finite difference/finite element of the immersed boundary method (submitted). 2013.

[4] R. Löhner, J. Cebral, O. Soto, P. Yim, and J.E. Burgess. Applications of patient-specific cfd in medicine and life sciences. *International journal for numerical methods in fluids*, 43(6-7):637–650, 2003.

[5] F.M. White. *Viscous Fluid Flow*. McGraw-Hill, New York, 2nd edition, 1991.

[6] B. Wu, A. Van Hirtum, and X.Y. Luo. Pressure driven steady flow in constricted channels of different cross section shapes. *International Journal of Applied Mechanics*, 5(1):1–18, 2013.